

**Reynolds Number and Drag**  
***A Comprehensive Analysis of Fluid Dynamics Over a Circular Post***  
Annie Gao, Hannah Singer, Sarah Fischer, Adam Laycock

## Abstract

The study of fluid dynamics is relevant to countless engineering applications, from pipe systems to aerial flight. This project introduces fundamental concepts of fluid dynamics using numerical simulations. It explores velocity fields and drag by analyzing the two-dimensional, incompressible flow around a spherical post within a bounded channel. All numerical simulations were performed in COMSOL—a software used for the study of computational fluid dynamics—to investigate drag forces and flow patterns across Reynolds numbers ranging from 0.1 to 100. As Reynolds numbers increase, flow transitions from laminar to unstable - this simulated behavior is discussed in detail. Velocity profile diagrams for various increasing Reynolds numbers are also produced and analyzed to validate results. The findings reveal the relationship between the Reynolds number and drag and illustrate the transition from a steady, laminar flow to an unsteady flow regime. Further analysis identifies sources of error and validates simulation results against known theories including Stokes' and the behavior of flowing fluids and their drag coefficients.

## Introduction

Before analyzing specific simulations, it is necessary to have a basic understanding of the fundamental principles and concepts at play.

Understanding the Reynolds number ( $Re$ ) and its implications is essential to understanding this project. The Reynolds number represents the ratio between inertial forces and viscous forces. It is calculated by multiplying an object's length ( $L$ ), the average velocity of the flow( $v$ ), and the fluid density ( $\rho$ ), and dividing by the fluid viscosity ( $\mu$ ). The resulting formula is:

$$Re = \frac{\rho v L}{\mu}$$

Systems with high Reynolds numbers correspond to scenarios where inertial forces dominate, resulting in turbulent flows. Conversely, low Reynolds numbers are characterized by the dominance of viscous forces, resulting in laminar flows. The project will mainly focus on laminar flow and the transition into turbulence [1].

The drag force an object experiences in any given flow is dependent upon a multitude of characteristics including shape, inclination, and flow conditions. An object's coefficient of drag encapsulates all of these properties for a given set of conditions. The drag coefficient ( $C_d$ ) is equal to the drag ( $D$ ) divided by the quantity: fluid density ( $\rho$ ) times half the velocity ( $v$ ) squared times the reference area ( $A$ ) [2].

$$C_d = \frac{2D}{\rho A v^2}$$

With a basic understanding of the Reynolds number and the drag coefficient established, we can now move on to the procedures of our simulations, which explore the relationship between these quantities in fluid flow.

## Methods

COMSOL software produced the simulations for this project. We considered a two-dimensional, Newtonian, and incompressible flow through a channel containing a circular post. The object is assumed to sit static in a channel. Cartesian coordinates were chosen with an x-y coordinate system. We chose to avoid three-dimensional simulations due to their extended computational time for the sake of our study and opted to gather data points at more Reynolds numbers instead.

### *Geometry and Domain*

The computational domain for this simulation was designed to be a rectangular channel to simplify the analysis and allow for computational efficiency. The geometry consisted of a circular post subtracted from a two-dimensional rectangular channel. The channel's height and width were set to 70 and 7 times the diameter of the circular post, respectively. These dimensions were chosen to avoid complex interactions between the channel and the object, allowing for an accurate representation of the flow around the circular post. The circular diameter was 0.1 m, height was 1.4 m, and width was 14 m. The circular post was positioned ( $\frac{1}{2}W$ ,  $\frac{1}{2}H$ ), with W and H being the width and height of the channel, respectively. The channel was positioned with the origin at the bottom left corner, ensuring that the flow downstream of the circular post is more visible and has more channel width to visualize.

### *Boundary Conditions*

The boundary conditions for the geometry were defined as follows. The inlet was designated as the left edge of the rectangle, where a parabolic velocity profile was inputted to simulate laminar flow. The outlet was designated as the right edge of the rectangle, and a zero-pressure boundary condition was applied so that the fluid could freely exit the boundaries. This inlet-outlet configuration allowed for the flow to move in the positive x-direction through the channel and around the circular post. The top and bottom edges were treated as no-slip boundaries, ensuring that the fluid velocity at these surfaces was zero relative to the channel walls. Finally, the circular post surface was also treated as a no-slip boundary.

### *Fluid Properties and Material Selection*

Water was used for this simulation, with the standard properties for density ( $1000 \text{ [g/m}^3\text{]}$ ) and dynamic viscosity ( $0.001 \text{ [Pa*s]}$ ). The flow regime was assumed to be stationary for  $Re=0.1$  to 10 and time-dependent for  $Re=10$  to 100.

### *Mesh Generation/Validation*

A computational mesh of normal density was generated. The mesh was concentrated near the circular post in order to accurately reproduce boundary layer effects and drag forces. It was less concentrated in the broader rectangular region for computational efficiency. To validate the results, we needed to ensure that the results were not completely dependent on the meshing we used. The [mesh validation](#) can be found in the appendix. To do this, we conducted six additional simulations. The additional experiments were done by using a “finer” and “coarser” mesh at Reynolds numbers 1, 10, and 100. The purpose of this was to ensure similar results occurred when using different meshes. We compared our results by comparing whether the flows at each Reynolds numbers were relatively consistent (ie. if a flow was laminar at a normal mesh at Reynolds number 1, it should also be laminar at the finer and coarser meshes). Additionally, we compared the coefficients of drag at each Reynolds number to ensure the values were similar. We

allowed for a 5 percent error. None of the resulting differences in the coefficients of drag were greater than 5 percent, and the velocity profiles all demonstrated the same flows as the tests at their Reynolds numbers with different meshes, so the mesh is considered valid. The error was calculated using the formula:

$$\% \text{ error} = \frac{C_{\text{Coarse/Fine}} - C_{\text{normal}}}{C_{\text{normal}}} \times 100$$

### Parameters

The Reynolds number was used as the primary parameter, as defined by  $Re = \frac{\rho v L}{\mu}$ . For each case, the inlet velocity was adjusted to achieve the desired Reynolds number. In global variables, a variable for velocity was set up to produce a parabolic velocity profile at the inlet in the x-direction, such that entrance and end effects are negligible. There was no velocity field generated in the y-direction at the inlet. The density was set to 1000 [ $\text{g}/\text{m}^3$ ], diameter to 0.2 [m], and dynamic viscosity to 0.001 [ $\text{Pa}\cdot\text{s}$ ]. These were unchanged throughout the iterations of simulations - the velocity was the only variable changed to achieve both the velocity profile and the drag coefficient plot for each chosen Reynolds Number.

### Simulation Procedure and Analysis

First, the geometry, boundary conditions, material properties, and global parameters and variables were configured. Next, a mesh was built to ensure convergence of results for drag force computation. The study was computed to produce the resulting velocity profile and streamlines, with a focus on the behavior immediately downstream the circular post. A line integral was set up to compute and output a table and plot of drag coefficients as well as drag coefficient over time. A stationary analysis was performed for lower Reynolds number up until  $\sim 10$ , and then a time dependent study was performed for up to  $Re=100$ . A parameter sweep was used to step Reynolds numbers and compute their drag coefficients in order to produce the Drag as a Function of Reynolds Number plot [[Figure 4](#)].

## Results

The results of the COMSOL simulations may be found in the appendix of this paper. The drag coefficient on the post inside the channel for Reynolds numbers ranging from 0.1 to 100 was plotted against time, and these figures can be found in the Appendix section along with their velocity profiles and streamlines. Drag coefficients for some Re were also determined [[Figure 1](#)].

Re	Coefficient of Drag
0.1	174.82
0.2	87.93
0.3	58.80
0.4	44.23
0.5	35.49
0.6	29.68
0.8	22.44
1	18.14

Re	Coefficient of Drag
2	9.63
4	5.44
8	3.25
10	2.77
20	1.72
40	1.10
60	0.84

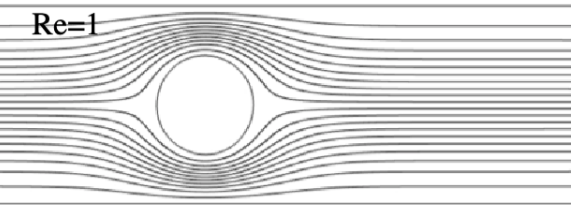
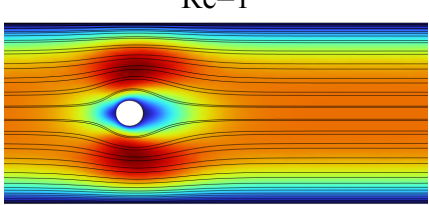
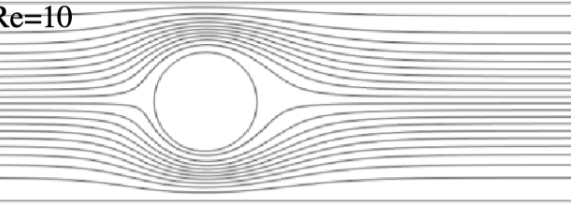
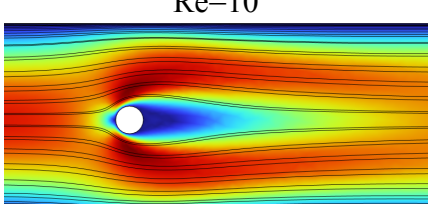
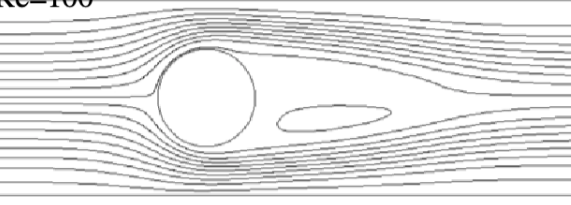
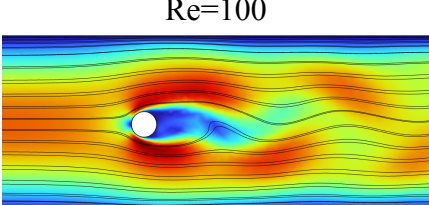
*Figure 1: Table of coefficient of drag values for a range of Reynolds numbers*

#### Transition Regime, Stable and Unstable Flow

The drag coefficient scales differently depending on the regime of the flow. In lower Reynolds numbers, the drag coefficient scales inversely with the Reynolds number. The derivation and discussion of this, which is based on Stokes' Law, is discussed below in the section titled "Comparison to Stokes' Law." As Reynolds number increases, the flow becomes more complex, as inertial forces dominate more significantly. In this regime, the drag coefficient decreases less sharply compared to that of smaller Reynolds numbers. The drag coefficient plotted against time will also oscillate—as visible in figures located in the Appendix—due to unsteady flow phenomena, such as vortex shedding.

The value of the Reynolds number for which the flow inside the channel became unstable—directly downstream of the circular post—was simulated to be around 60 (with a velocity of 0.6 m/s) under our chosen parameters and dimensions. This is when the unsteady flow phenomena becomes visible downstream of the circular post, and this velocity profile is visible in the Appendix table for Re=60.

The table below [[Figure 2](#)] provides a side by side comparison of velocity profiles at three Reynolds numbers from the figures provided to us and our own experimental results. We opted to keep the color underlaid with the streamlines to visualize the areas where velocity is the highest in magnitude (the redder areas).

Figures Given	Experimental Results
	
	
	

*Figure 2: Velocity profile comparisons of provided streamlines and our simulated streamlines for three Reynolds numbers in transitioning regimes.*

As shown above [[Figure 2](#)], at low Reynolds numbers ( $Re=1$ ) there is stable flow and symmetric streamlines upstream and downstream around the circular post. At  $Re=10$  and higher (with increasing simulated velocity) up until the transition to an unstable regime, the flow remains stable, but the downstream streamlines begin to take on a more pronounced wing-like shape. At  $Re=100$ , the flow is unstable.

Our results also demonstrated the relationship between the drag coefficient and the Reynolds number, as visible from our data points (blue) overlaid on with the provided graph [[Figure 3](#)] [[Figure 4](#)]. Specifically, the drag coefficient exhibits a linear relationship with the Reynolds number only up to approximately  $Re=1$ ; beyond this range, the relationship becomes nonlinear as inertia effects grow more significant. Any slight deviations between our experimental results and the given graph are further discussed in the Sources of Error section [[Figure 3](#)].

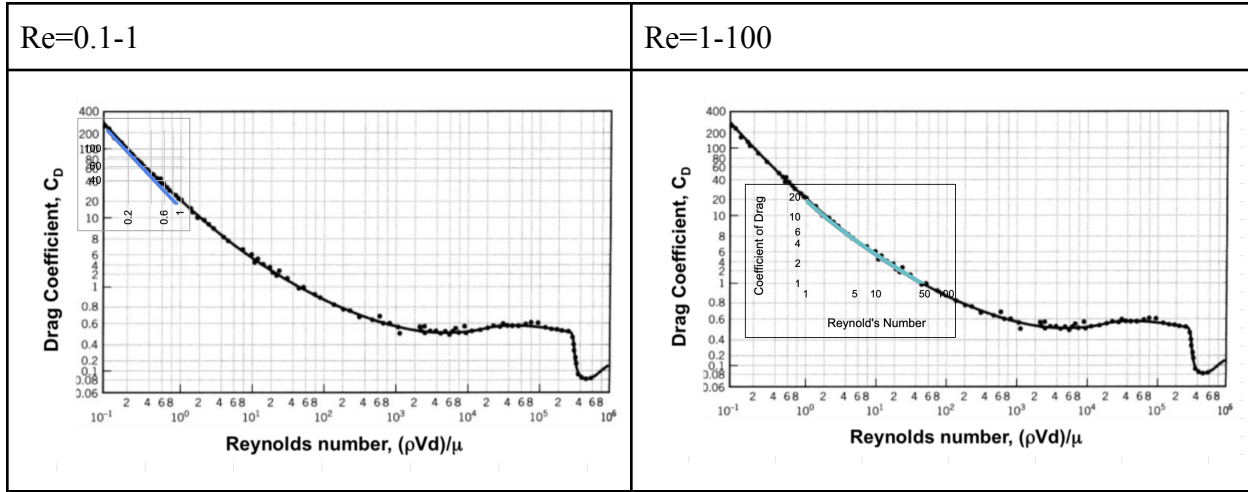


*Figure 3: Overlaid comparison of drag coefficient versus Reynolds number for Reynolds numbers from 0.1-10 and 1 to 100.*

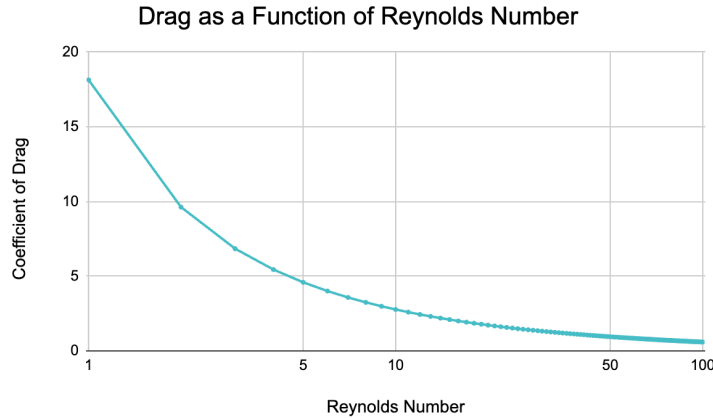


*Figure 4: Drag coefficient as a function of Reynolds numbers.*

Again, the figure above confirms the nature of how the drag coefficient and Reynolds number are related [Figure 4]. As inertial effects become significant, flow separation can occur.

Flow separation occurs when the flow is unable to follow the body it is flowing around, so it separates from the body. If the body is smooth and the viscosity of the fluid is large enough that it dominates over inertial forces, or in other words, if the Reynolds number is low, the flow will follow the outline of the body. If there are sharp transitions or the Reynolds number gets too large (i.e., inertial forces dominate) then flow separation occurs, which results in unstable flow and turbulence [3]. This correlates with what we saw in the results of our simulations, as higher Reynolds numbers resulted in unstable flow that did not closely follow the contours of our sphere. The visualizations above demonstrate this phenomenon with a separation bubble or dividing streamline, which is the contour that the flow actually ends up following. The simulations we performed similarly have contour bubbles and, more evidently shown below, have dividing streamlines. The streamlines of the simulations with higher Reynolds numbers have streamlines that detach from the surface of the sphere and either don't become uniform until soon before the outlet, or don't become uniform at all. This separation results in unstable flow.

It is important to note the distinction between turbulent flow and unstable flow. Unstable does not automatically signal turbulent flow. A flow can be unstable and still maintain a coherent, periodic structure, as visible in the fluctuations of drag coefficients over time in the Appendix figures.

### Comparison to Stokes' Law

The derivation for the drag coefficient given a known Reynolds number is as follows:

$$F_D = 6\pi\mu Rv, \text{ where } v \text{ is velocity around the sphere}$$

$$\begin{aligned} C_d &= \frac{F_D}{\frac{1}{2}\rho v^2 AR^2 \pi} \\ C_d &= \frac{6\pi\mu Rv}{\frac{1}{2}\rho v^2 \pi R^2} = \frac{12\mu}{\rho v R} = \frac{12}{Re}. \end{aligned}$$

Note that the numerator in the drag coefficient derivation for a given Reynolds number uses 12 because our radius was considered. If diameter was used instead, it would be  $C_d = \frac{24}{Re}$ . The resulting drag coefficient from our stationary simulations from Reynolds number of 1 to 10 is plotted against the Stokes' Law's/Flow's theoretical values [Figure 5].

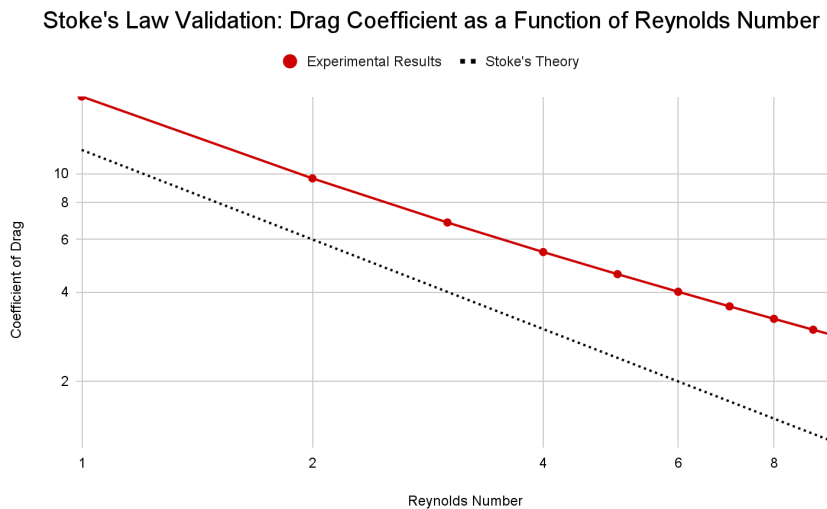


Figure 5: A validation of experimental results with Stoke's Theory. Drag coefficient as a function of Reynolds number for Reynolds numbers from 1-10.

As shown above, Stokes' Law underpredicts the simulated coefficients of drag [Figure 5] produced by our model. At a Reynolds number of 1, for instance, Stokes' Law predicts a drag that is 10 percent lower. Stokes' predicts lower coefficients of drag because it assumes idealized conditions, which includes steady, incompressible, and pure laminar flow with negligible inertial effects. These assumptions only suit a regime of creeping flow, that is, Reynolds numbers  $< 1$ . Meanwhile, the COMSOL model takes those behaviors into account. Even at lower Reynolds numbers, there can still be minor inertial effects. The boundary and mesh computations also consider localized variations in flow, which Stokes' theory does not. Despite this, our COMSOL model is not without limitations. We modeled the problem with a 2D Cartesian coordinate system, which is a simplification of the true 3-dimensional, axisymmetric nature of the problem.

Further consequences of this coordinate system simplification is discussed in the “Sources of Error” section.

### Sources of Error

There are several potential sources of error to discuss, the first of which is the channel dimensions. Although the boundaries were set much larger than the diameter of the circular post, they may still influence the flow. If the boundaries and walls are not sufficiently far from the post, they could interfere with the flow field, introducing unintended unsteadiness. This would affect the drag coefficient.

As mentioned above, using a Cartesian coordinate system rather than a cylindrical one also impacted the accuracy of our simulated drag coefficients across varying Reynolds numbers. In a Cartesian system, the mesh near the circular post would have to use straight-edged geometry to represent a curved boundary. This, coupled with the use of less refined mesh, can affect boundary layers and the flow behavior. Additionally, a cylindrical coordinate system may have been more computationally efficient given that the object in the channel was circular, aligning naturally with the geometry of the flow.

In a broader context, two-dimensional Cartesian geometry assumes uniformity in the third dimension, but the actual flow around a sphere behaves differently. The differing coordinate system assumptions affect the velocity distribution, and, consequently, the drag. Thus, using a r-z coordinate system would have been more accurate in producing correct drag coefficients for the given parameters.

### **Conclusion**

In summary, this paper explored the relationship between Reynolds number and the drag coefficient by simulating fluid flow over a circular post in a channel and capturing the transition from laminar flow to unstable regimes. Our experimental results were validated by comparison to given graphs and theories including Stoke's, and sources of error were discussed. This paper also explored the COMSOL software, which revealed much about the nature of computation fluid dynamic simulations.

### **Additional Study/Exploration: Lift on an Airfoil**

Lift is an upward force that an object experiences in a moving fluid. Similar to drag, it is dependent upon shape, inclination, and flow conditions. An object's lift coefficient encapsulates all of these properties for a given set of conditions. The lift coefficient ( $C_L$ ) is equal to the lift ( $L$ ) divided by the quantity: fluid density ( $\rho$ ) times half the velocity ( $v$ ) squared times the reference area ( $A$ )[4].

$$C_L = \frac{2L}{\rho A v^2}$$

In the simulations of the circular post, no lift was observed due to the symmetry of the post. To explore the phenomenon of lift, we ran similar simulations on an airfoil at various angles and recorded the lift coefficients, as well as the drag coefficients and velocity profiles. While there are other components of aircrafts that are used to induce lift such as wing flaps, we only examined flow around an airfoil. In order to best approximate the conditions that an airfoil

experiences during flight, we made some significant modifications to the study. Namely, we changed the flow medium to air and adjusted the Reynolds number to  $10^7$ .

Lift is a concept that is heavily debated and often misunderstood. Take an airfoil, for example: the intuitive explanation for many is that the shape of an airfoil causes air to be pushed down, therefore pushing the airfoil up due to Newton's third law. While this is partially true, it is an incomplete explanation. Along with a basic understanding of linear momentum, NASA's definition of lift is helpful in understanding the complete picture: "lift is a force generated by turning a moving fluid" [5]. When the windward side of the airfoil pushes the air down or "turns" it, the air's downward velocity (and momentum) increases. Momentum must be conserved, so the airfoil's upward momentum must increase by that same magnitude. However, the leeward side of the airfoil must also be considered. As seen in [Figure 6], the air that flows above the airfoil curves down to match its profile. Due to its viscosity, a thin boundary layer of air is created along the surface of the foil in which velocity is essentially 0. This allows air to flow smoothly and trace the downward curve of the airfoil, again increasing its downward momentum. Because the air is being pulled down by the airfoil, the airfoil must be pulled up by the air, resulting in additional lift.

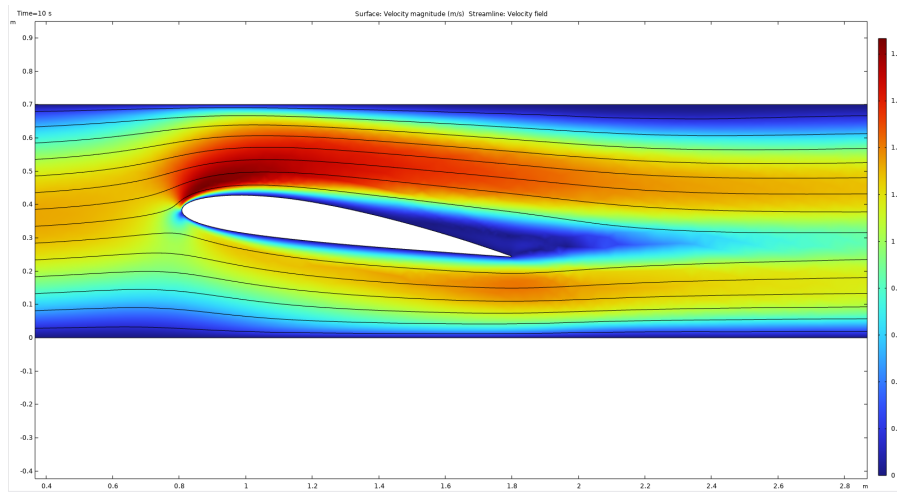


*Figure 6: Airfoil at 8 degrees. Velocity streamline curves around airfoil.*

During different phases of flight, an aircraft will have different angles of attack (AOA) and experience different amounts of lift. While at cruising altitude, most aircrafts will maintain an AOA of 2-5 degrees. During ascent, this value can increase to about 8-12 degrees, consequently increasing the lift. As the angle of attack continues to increase, lift will continue to increase until a critical AOA is reached (usually around 17 degrees). At the critical angle the air that goes over the airfoil can no longer follow the descent of the airfoil's shape [Figure 7]. This disrupts the boundary layer and creates a separation bubble in which there is unstable or turbulent flow. This flow significantly reduces the amount of air being redirected downwards, resulting in a dramatic loss of lift. This phenomenon is known as a stall.

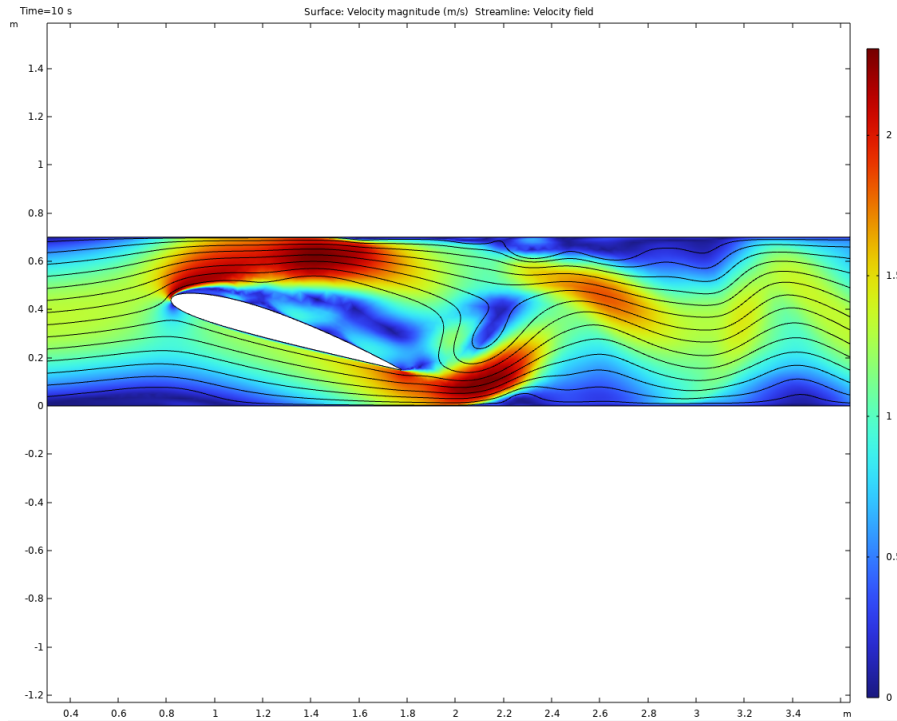


*Figure 7: 17 degree AOA. Boundary layer replaced by turbulent separation bubble resulting in a stall.*

Our simulations confirmed our understanding of lift and reinforced our understanding of drag, as the lift coefficient increased as we increased the angle of attack (seen [here](#) in appendix). When we reached higher angles of attack, however, our lift coefficient did not seem to converge with time. For instance, at 12 degrees, the lift coefficient was oscillating and growing in amplitude but it still had a clear midline at approximately 11 [1/m]. At 17 degrees, the oscillation was much more chaotic and did not seem to approach a single value. This may be directly caused by the fact that the airfoil was experiencing a stall, or it could be due to issues with our model and/or the simulation software. Regardless, the velocity profile plot demonstrates what we expected: a turbulent separation bubble hinders the airfoil's ability to turn the moving fluid.

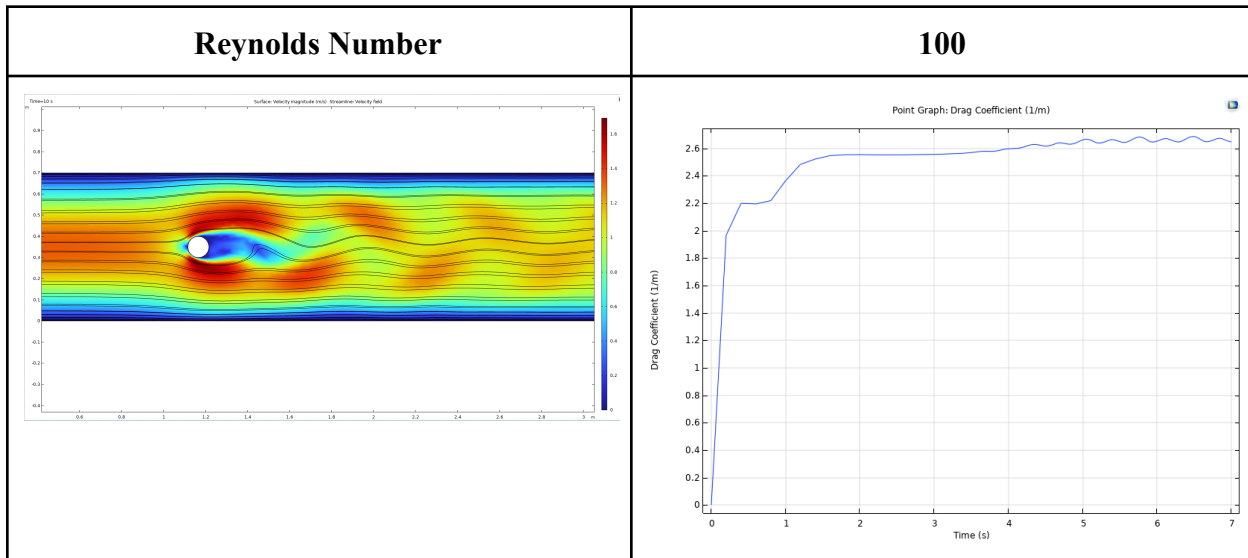
These simulations expanded upon our findings from the previous study by exploring the relationship between the orientation of an object and the drag and lift it experiences. They also demonstrated the importance of accounting for the leeward side of a given object when analyzing the causes of lift. This helps us consider real world applications and design measures taken to induce and maintain lift in relevant scenarios.

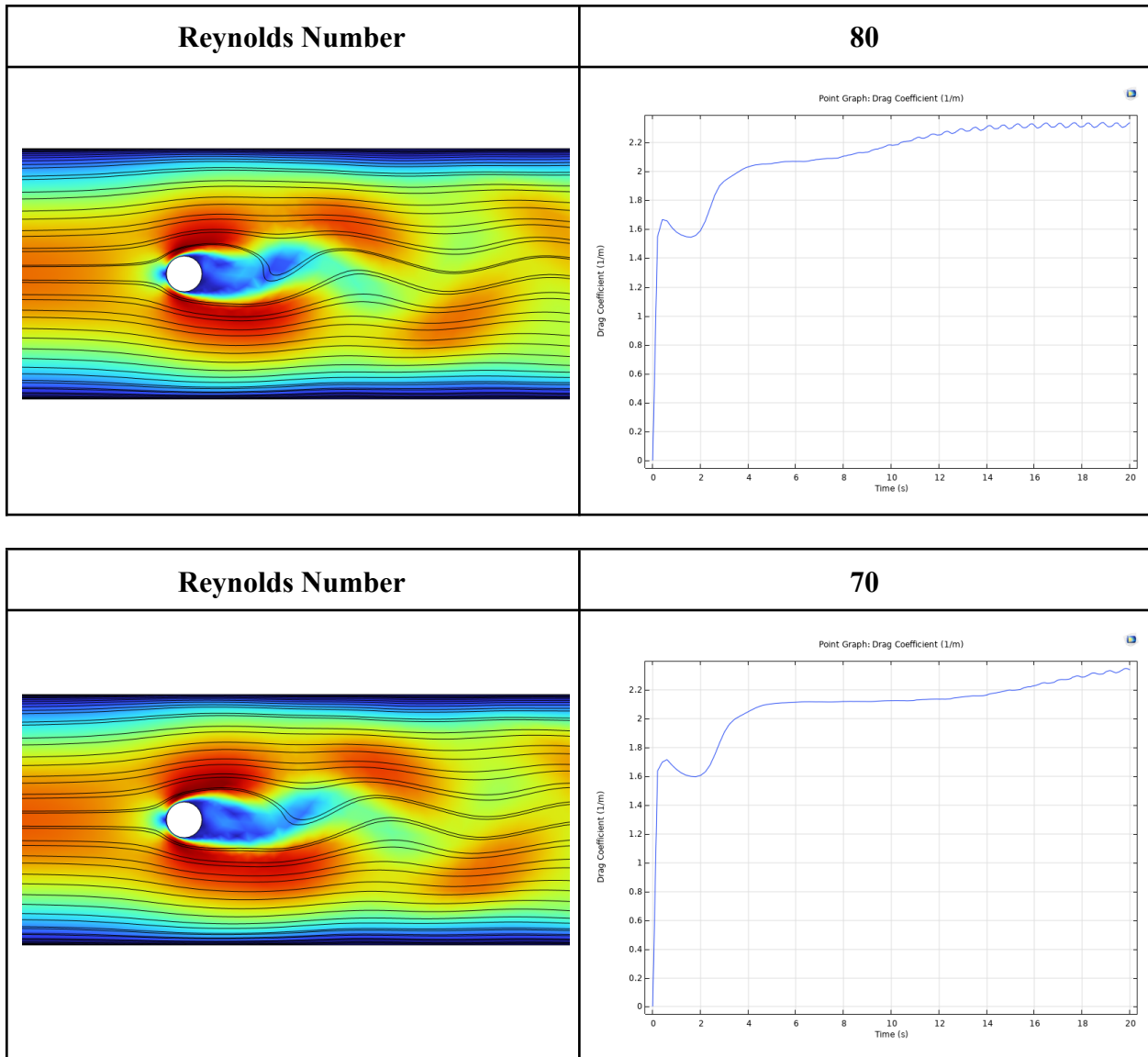
## References

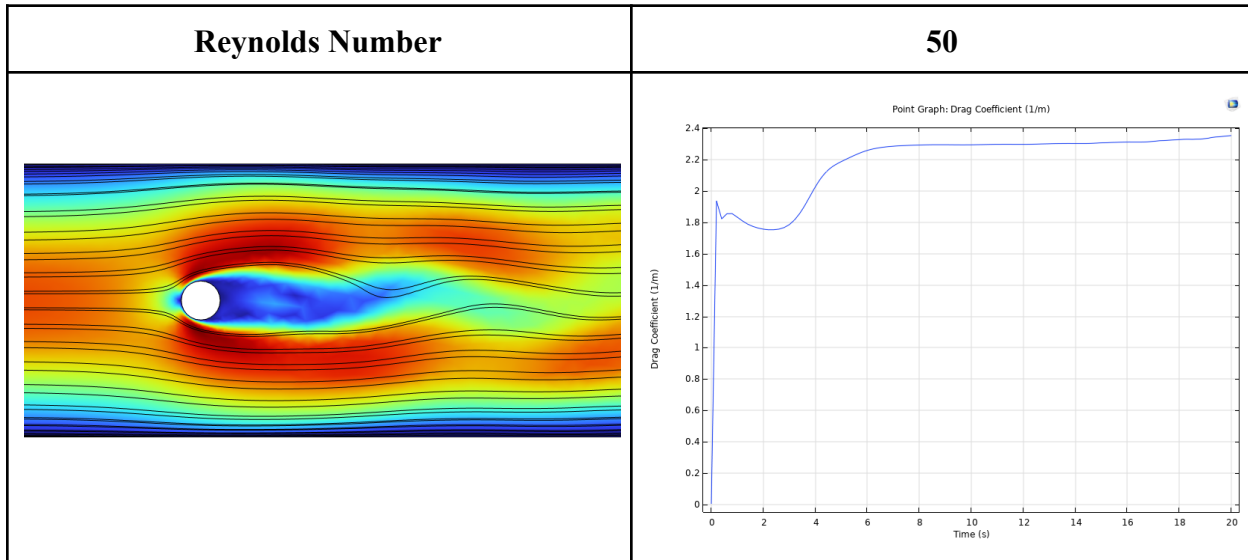
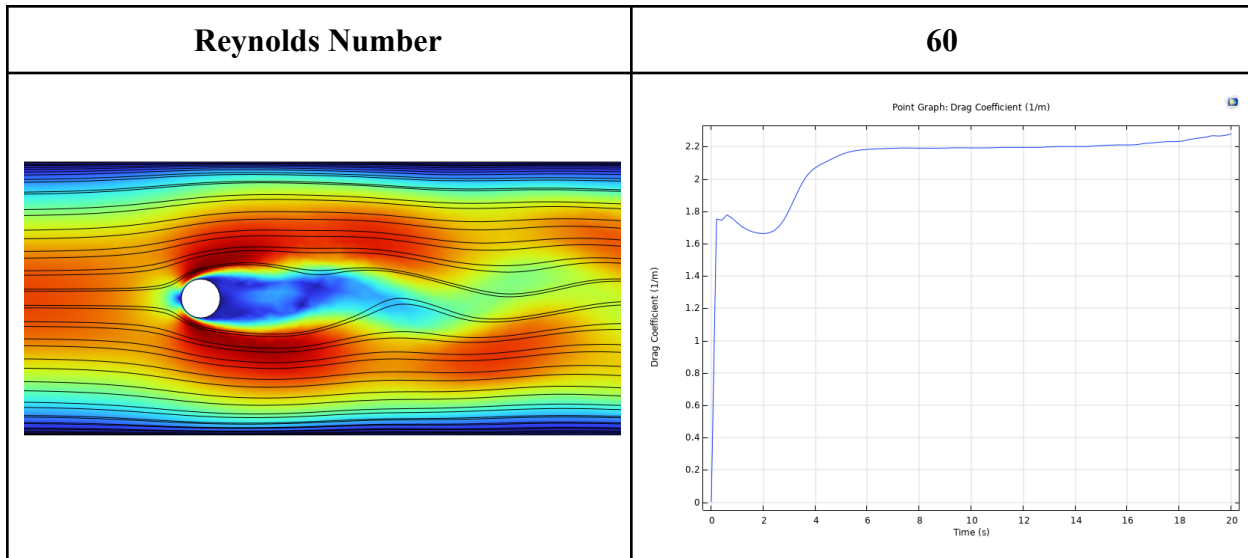
- (1) *Reynolds Number | Definition, Calculation & Examples | nuclear-power.com.* Nuclear Power. <https://www.nuclear-power.com/nuclear-engineering/fluid-dynamics/reynolds-number/> (accessed 2024-12-06).
- (2) *Drag Coefficient | Glenn Research Center | NASA.* Glenn Research Center | NASA. <https://www1.grc.nasa.gov/beginners-guide-to-aeronautics/drag-coefficient/> (accessed 2024-12-06).
- (3) *tec-science. Flow separation (boundary layer separation) | Tec-science.com.* <https://www.tec-science.com/mechanics/gases-and-liquids/flow-separation-boundary-layer-separation/> (accessed 2024-12-06).
- (4) *Benson, T. (n.d.). The Lift Coefficient | Www.grc.nasa.gov.* <https://www.grc.nasa.gov/www/k-12/VirtualAero/BottleRocket/airplane/liftco.html> (accessed 2024-12-08)
- (5) *Lift from Flow Turning. (2018). | Nasa.gov.* <https://www.grc.nasa.gov/WWW/k-12/airplane/right2.html> | (accessed 2024-12-08)

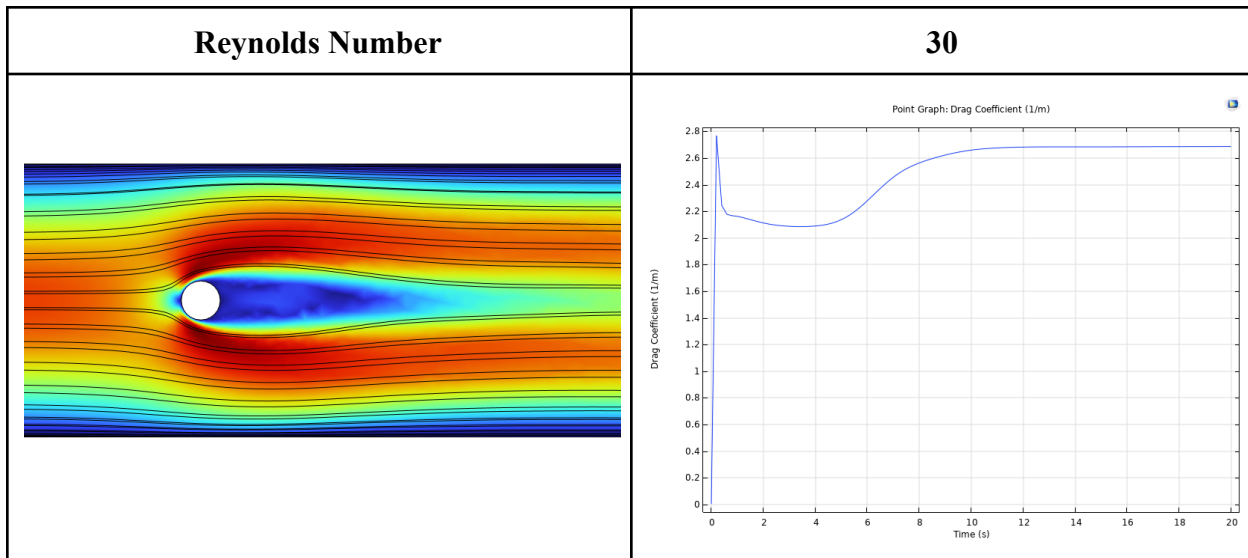
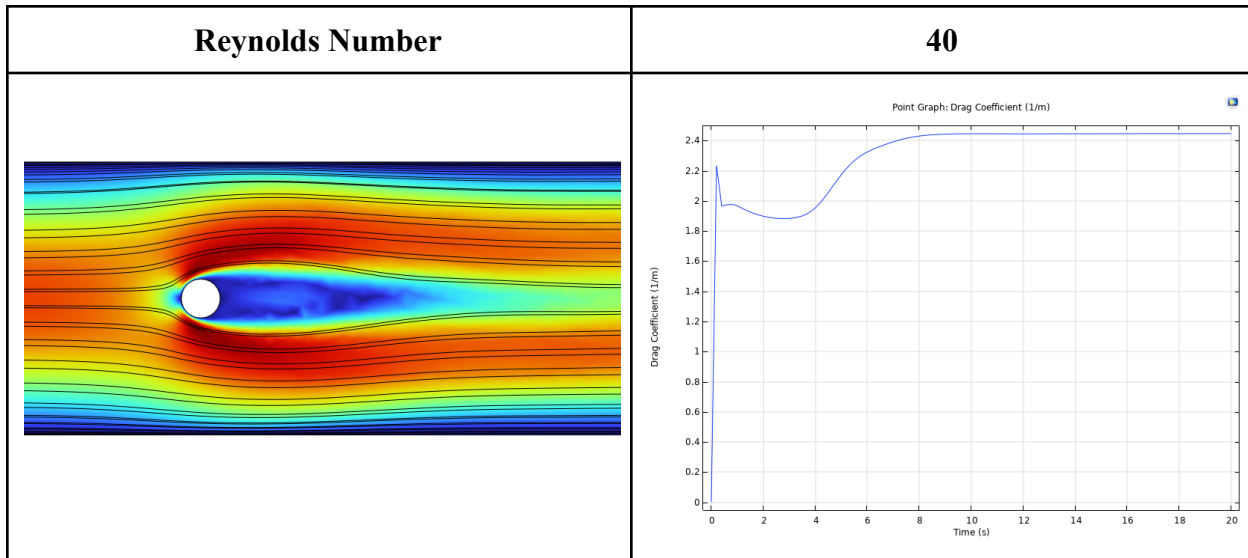
## Appendix

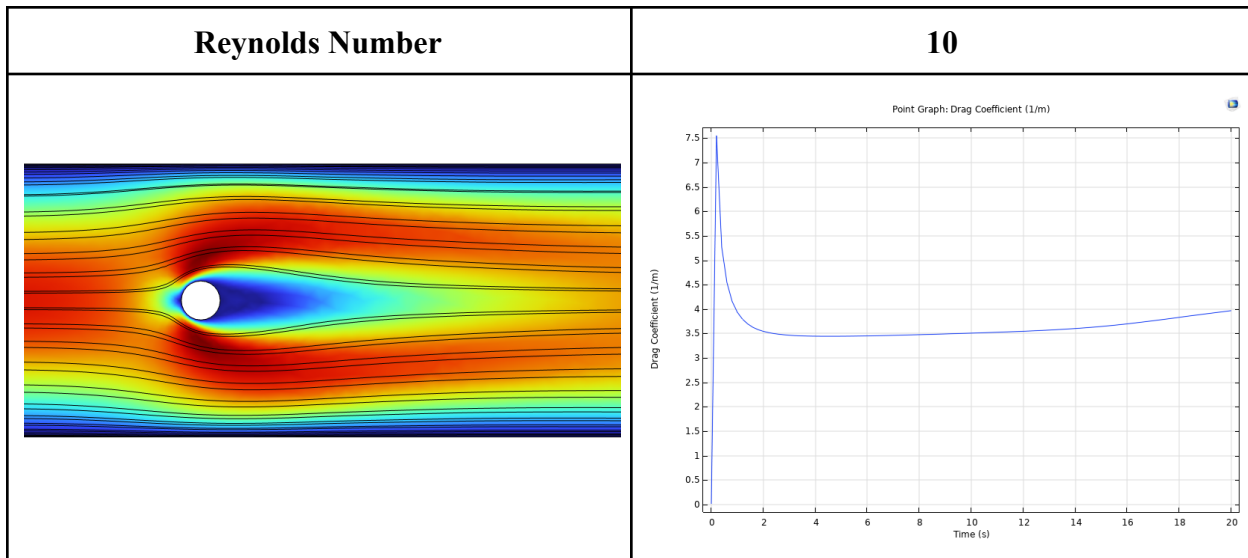
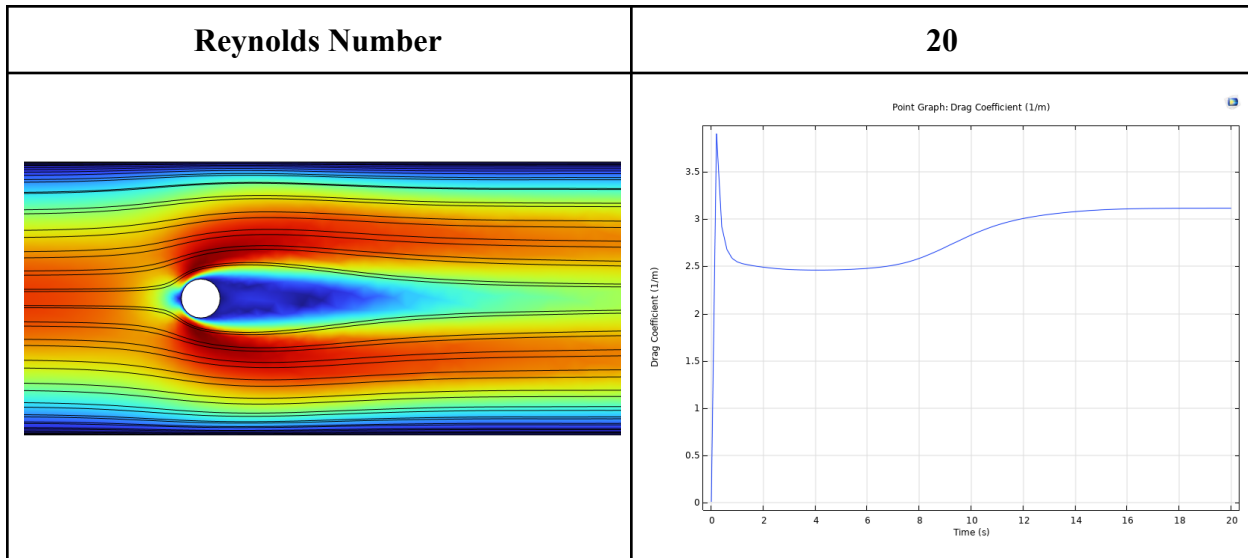
### Drag Coefficient Reynolds Numbers Simulations

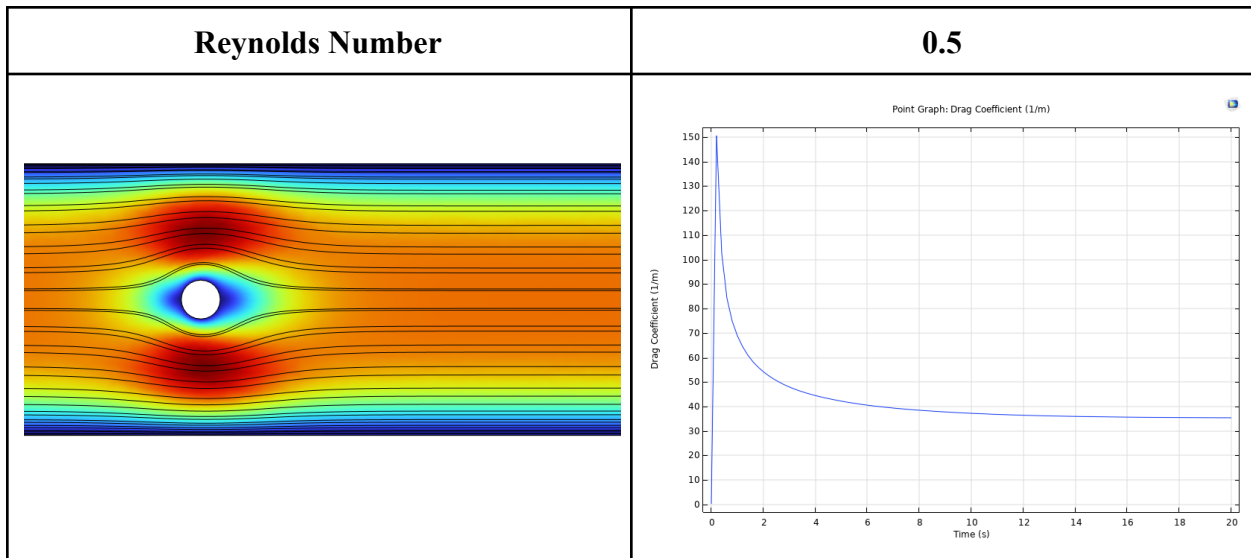
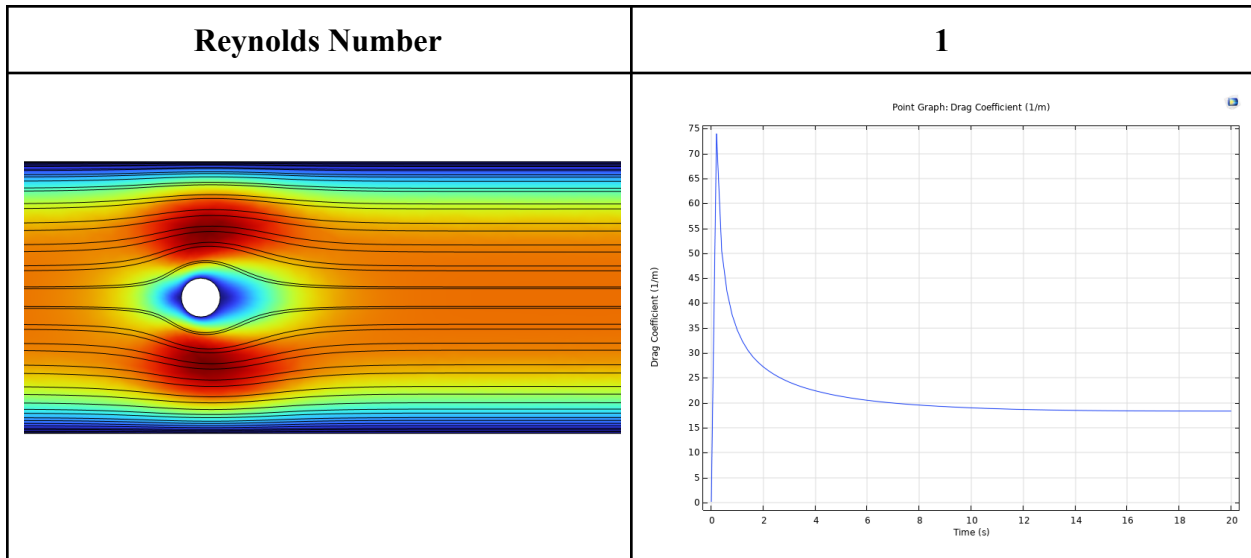


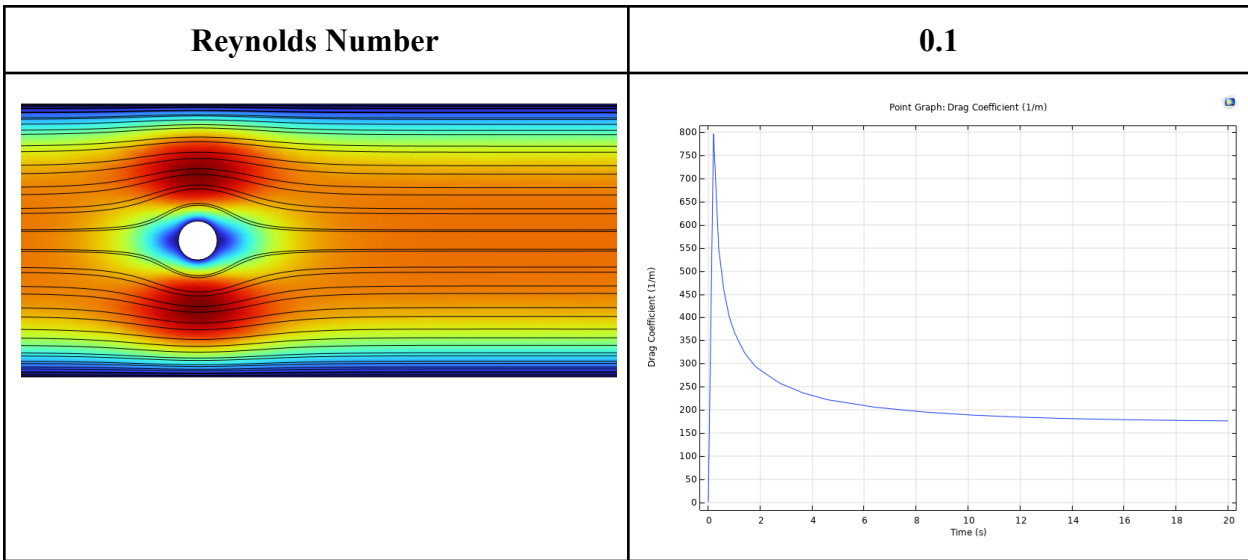




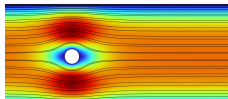
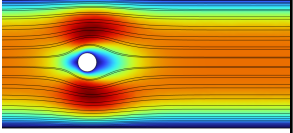
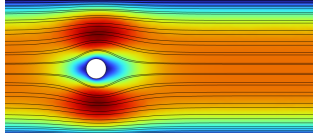
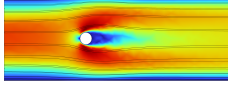
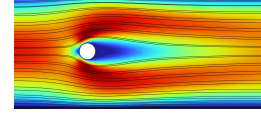
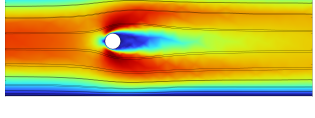
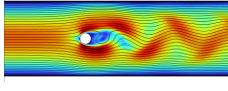
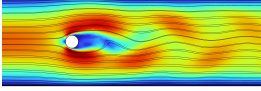
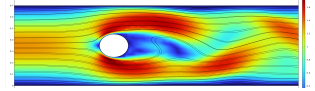




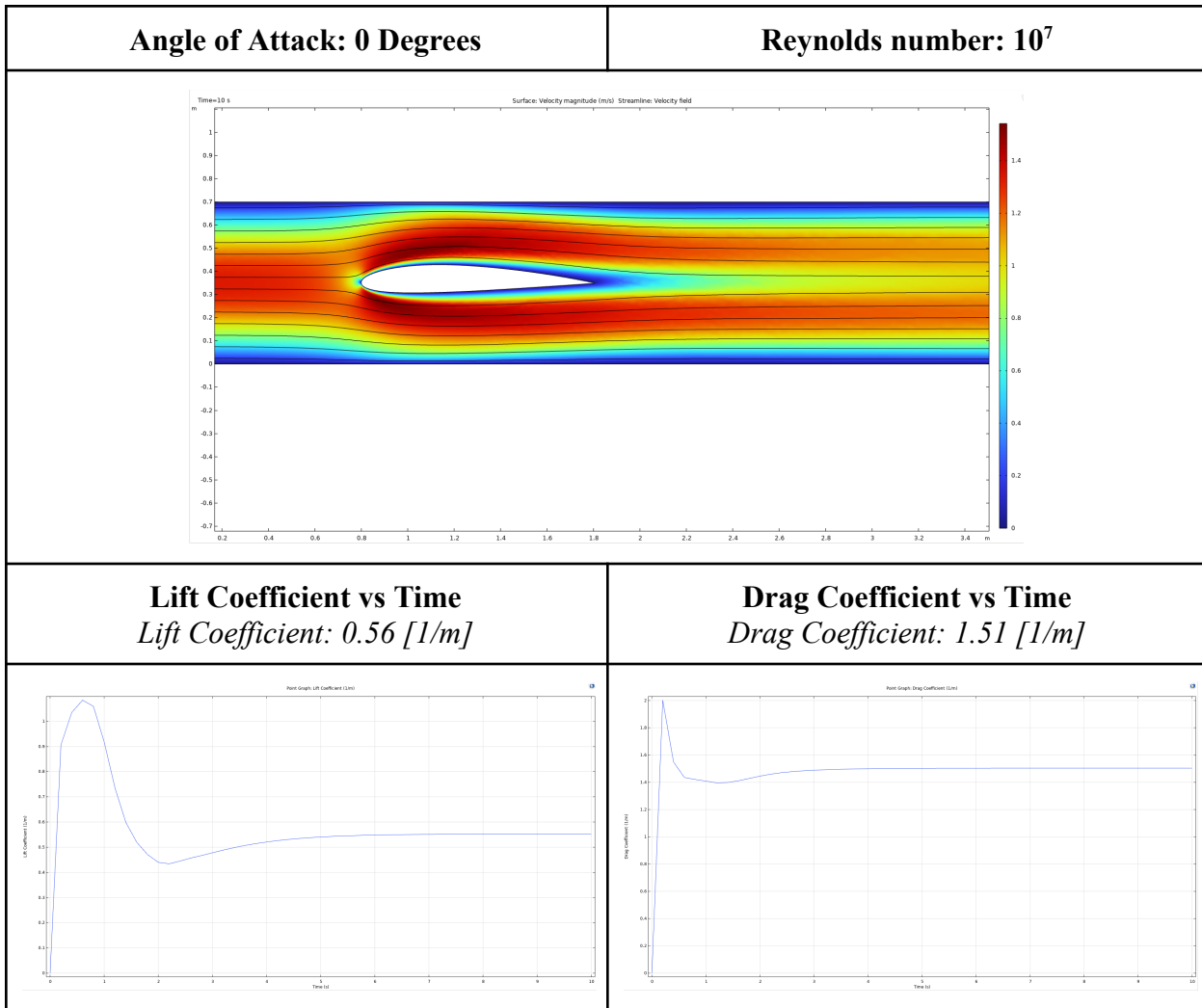




## Validation of Mesh

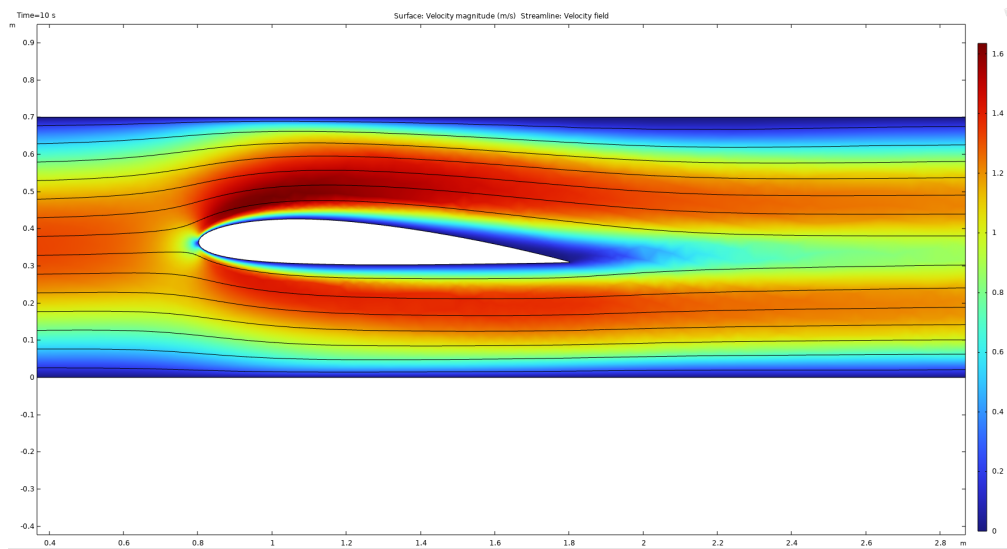
Comparisons of Velocity Profiles with Different Meshes				
Reynolds number	Finer Mesh	Normal Mesh	Coarser Mesh	Similar?
1				<i>Fine vs Normal: Yes Normal vs Coarse: Yes</i>
10				<i>Fine vs Normal: Yes Normal vs Coarse: Yes</i>
100				<i>Fine vs Normal: Yes Normal vs Coarse: Yes</i>

## Exploration Simulations



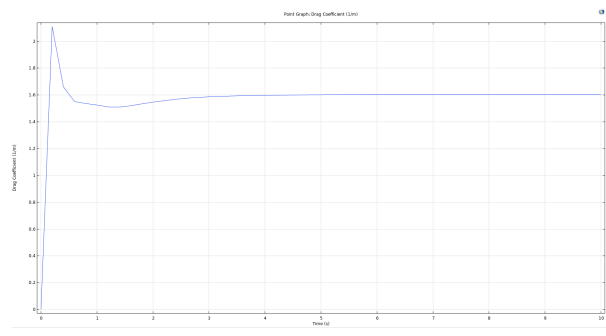
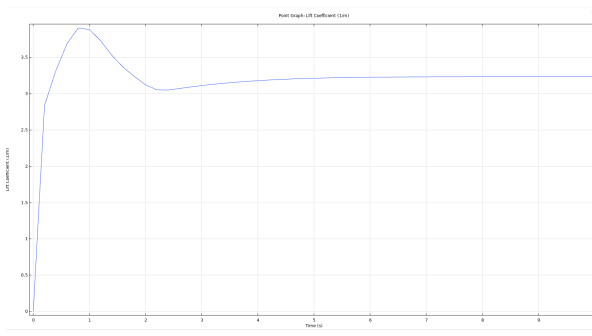
**Angle of Attack: 3 Degrees**

**Reynolds number:  $10^7$**



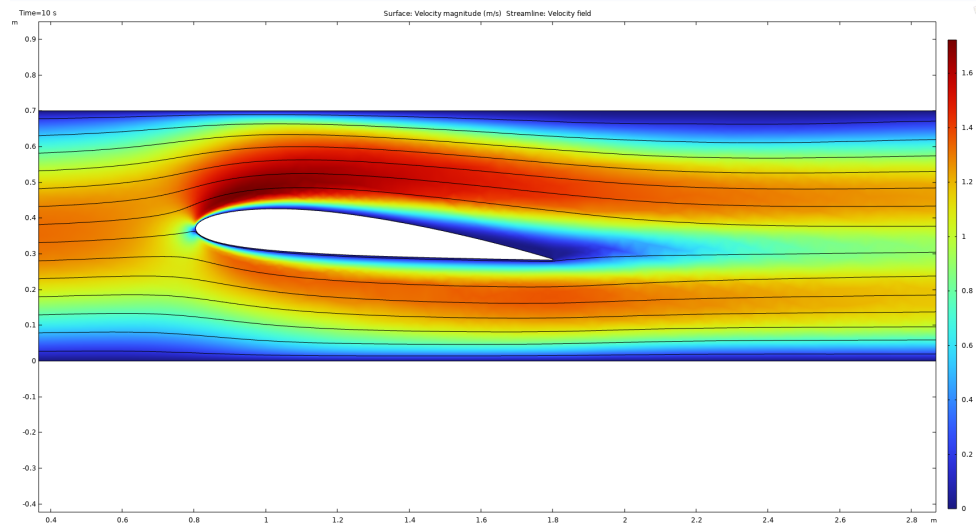
**Lift Coefficient vs Time**  
*Lift Coefficient: 3.20 [1/m]*

**Drag Coefficient vs Time**  
*Drag Coefficient: 1.60 [1/m]*



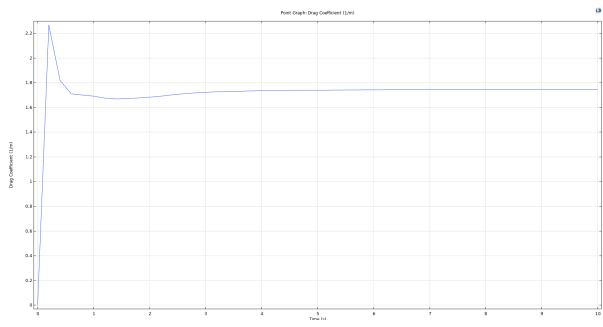
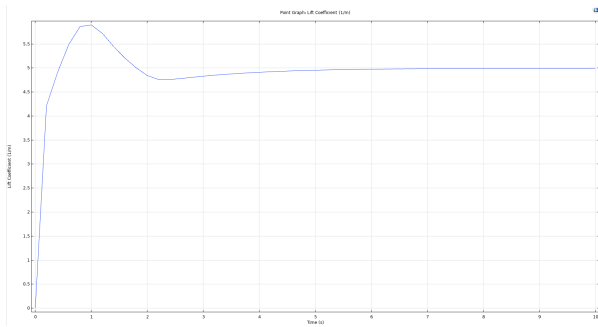
**Angle of Attack: 5 Degrees**

**Reynolds number:  $10^7$**



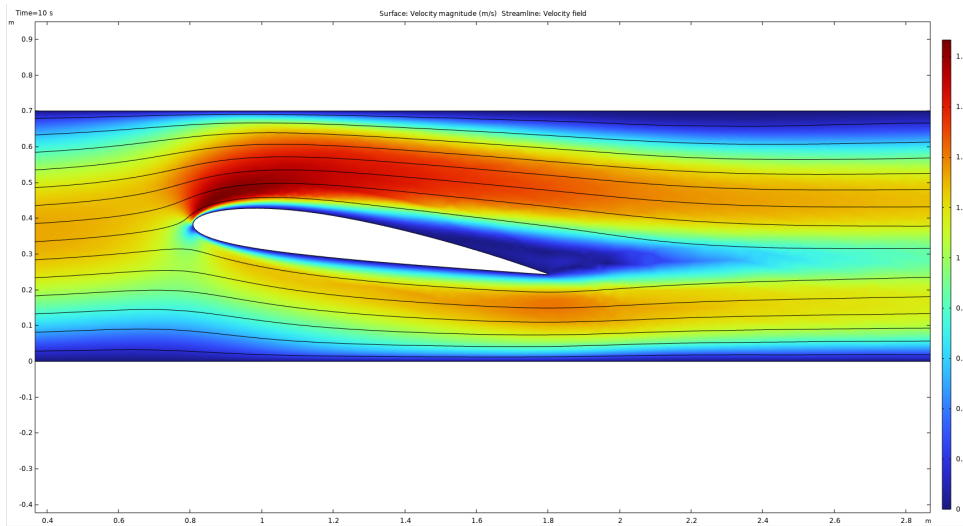
**Lift Coefficient vs Time**  
*Lift Coefficient: 5.00 [1/m]*

**Drag Coefficient vs Time**  
*Drag Coefficient: 1.76 [1/m]*



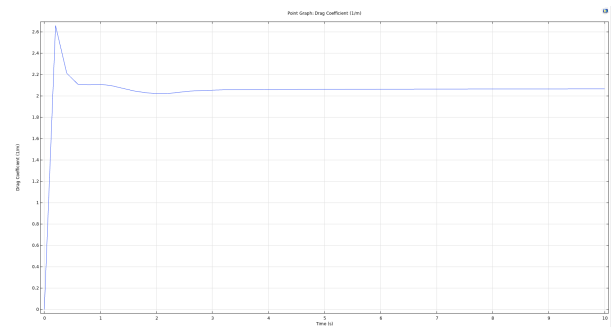
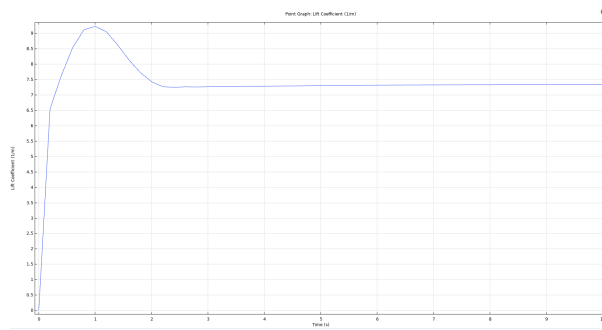
**Angle of Attack: 8 Degrees**

**Reynolds number:  $10^7$**



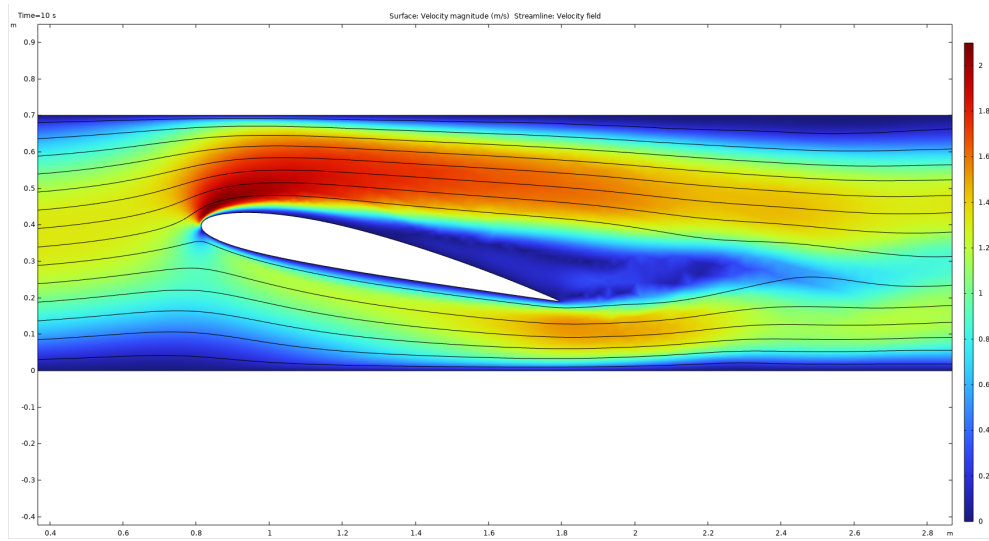
**Lift Coefficient vs Time**  
*Lift Coefficient: 7.40 [1/m]*

**Drag Coefficient vs Time**  
*Drag Coefficient: 2.05 [1/m]*



**Angle of Attack: 12 Degrees**

**Reynolds number:  $10^7$**

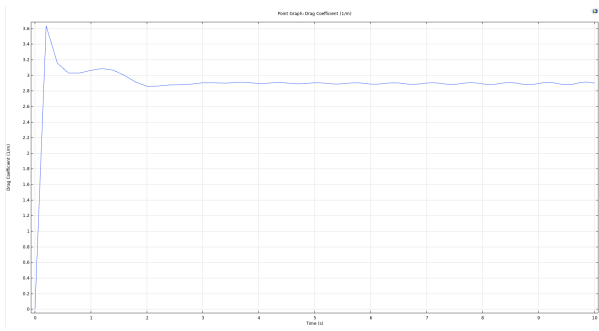
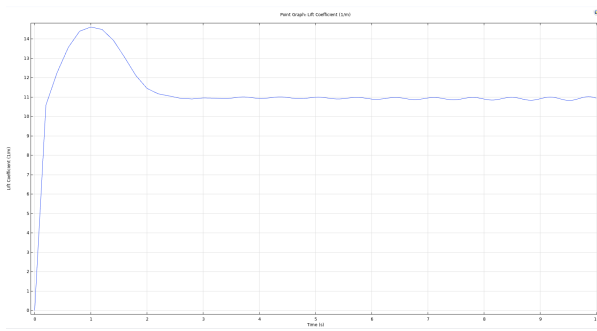


### Lift Coefficient vs Time

*Lift Coefficient: Oscillating around 11 [1/m],  
but increasing in amplitude  $\therefore$  will not  
converge*

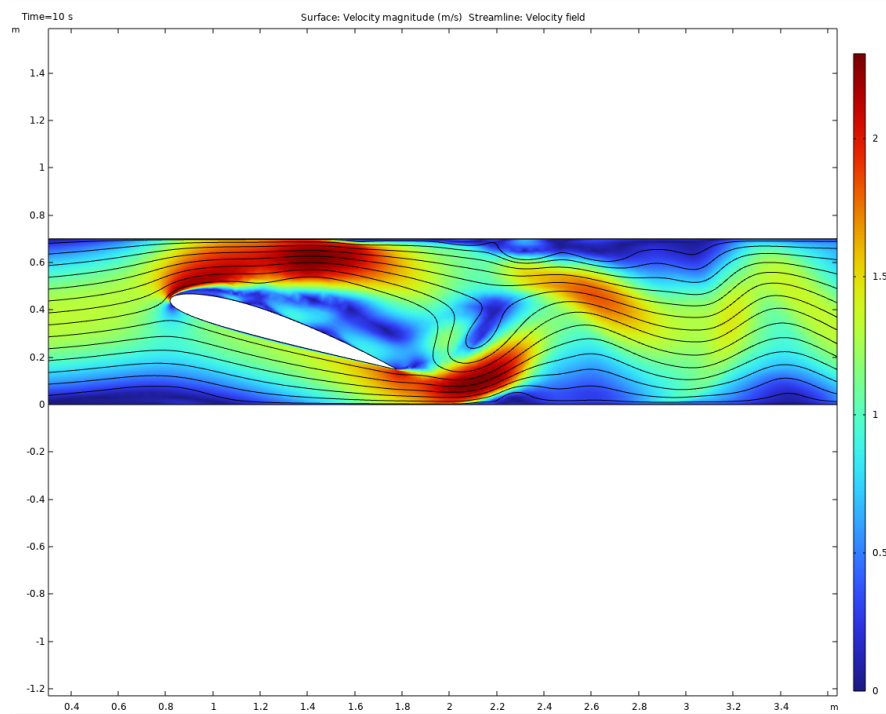
### Drag Coefficient vs Time

*Drag Coefficient: Oscillating around 2.9  
[1/m], but increasing in amplitude  $\therefore$  will not  
converge*



**Angle of Attack: 17 Degrees**

**Reynolds number:  $10^7$**



### Lift Coefficient vs Time

*Lift Coefficient: Roughly oscillating around 18 [1/m], but will not converge  $\therefore$  inconclusive*

### Drag Coefficient vs Time

*Drag Coefficient: Roughly oscillating around 5.75 [1/m], but will not converge  $\therefore$  inconclusive*

